Surfaces and Interfaces 21 (2020) 100672

Contents lists available at ScienceDirect

Surfaces and Interfaces

journal homepage: www.elsevier.com/locate/surfin

Hydrogen uptake performance of nanocomposites derived from Metal-Organic Framework (Cu-BTC) and metal decorated multi-walled carbon nanotubes (Ni@f-MWCNTs or Pd@f-MWCNTs)

Madhavi Konni, Anima S. Dadhich, Saratchandra Babu Mukkamala*

Nanoscience & Nanotechnology Laboratory, Department of Chemistry, Institute of Science, GITAM (Deemed University), Visakhapatnam, 530045, Andhra Pradesh, India

ARTICLE INFO

Keywords:
Functionalization
Metal decorated MWCNTs
Cu-BTC
Composites
Hydrogen uptake

ABSTRACT

The storage of hydrogen in solid materials has been investigated extensively in recent years for on-board vehicle applications for hydrogen fuel cell technology. Metal-Organic Frameworks (MOFs) are unique materials with novel porous structures suitable for reversible gas adsorption at low temperatures. Similarly, another porous material, carbon nanomaterial is also equally important in storage of hydrogen at room temperature. The Proposed new nanocomposites composed of metal-organic framework (Cu-BTC/HKUST-1) and metal-decorated multi-walled carbon nanotubes (Ni@f-MWCNTs or Pd@f-MWCNTs) are promising candidates for physisorption of hydrogen at low temperature and low pressures. Hence, Ni or Pd decorated MWCNTs were mixed with Cu-BTC at 95 °C to get the intercalated composite material. It was observed that Cu-BTC/Ni@f-MWCNTs and Cu-BTC/Pd@f-MWCNTs showed 4.68 and 5.31 wt% adsorption of hydrogen at 77 K and 70 bar, respectively. At 298 K and 70 bar pressure, the above two composites adsorbed 1.29 and 1.67 wt% of hydrogen. Enhanced hydrogen uptake of about 250-350% and 20-30% was observed at 298K by the synthesized composites compared to the Cu-BTC and metal decorated MWCNTs, respectively. Similarly, an enhancement of about 50-75% and 85-150% in the hydrogen adsorption capacity was observed at 77K for the composites compared to the pristine materials. The resultant enhanced hydrogen uptake by composites is probably due to the synergic effect between Cu-BTC and metal decorated MWCNTs.

1. Introduction

Hydrogen is one of the renewable and clean energy sources and most likely successor of conventional petroleum fuels [1,2]. The most challenging task for the success of the hydrogen economy is to develop efficient and cost-effective hydrogen storage material for the transport sector [3]. Therefore, the main goal in the hydrogen economy is to develop a suitable hydrogen storage medium to meet the U.S. Department of Energy (DOE) target of 5.5 wt% hydrogen by 2025 for onboard light-duty vehicles, material-handling equipment, and portable power applications [4]. Metal-Organic Frameworks (MOFs) are rapidly emerging as promising materials for gas storage applications owing to their exceptionally large surface area with tunable pore size and volume make them a good exclusive storage medium for hydrogen for clean energy applications [5]. Among 500,000 Metal-Organic Framework materials examined computationally for hydrogen storage, some compounds such as SNU-70, UMCM-9 and PCN-610/NU-100 were reported to have exhibited exceptional uptake capacity [6]. M_2(m-dobdc) (M = Co, Ni) is also known to have exhibited a high uptake capacity of 2.2 wt% at 77K and 1 bar [7]. However, among the large number of MOFs synthesized so far, Cu-BTC [Cu_3(benzene-1,3,5-tricarboxylate)$_2$(H_2O)$_3$], is one of the most studied open framework material for gas adsorption and storage applications [8]. Exceptionally high surface area (1721 cm^2/g) and microporosity (0.74 cm^3/g) makes Cu-BTC as one of the potential candidates for physisorption of gases [9]. Furthermore, at low pressures, Cu-BTC shows higher uptake of hydrogen compared to other MOFs which is desirable for storage applications [10]. But, MOFs tend to exhibit high hydrogen adsorption capacity only at low temperatures due to low adsorption enthalpy involved in physisorption, however, their properties can be further improved by tuning the sorption behavior by changing the chelating organic linkers, adding metals and making composites [11].

On the other hand, graphene, MWCNTs, metal and metal oxide decorated MWCNTs show higher hydrogen uptake behavior at room temperature [12–14]. Previous results show that the MWCNTs decorated with nanoparticles of Mg, Fe, Cu, Zn, Pd, Ni exhibit improved uptake capacities for hydrogen at room temperature and moderate pressures [15–19]. Many researchers have reported that the enhanced

* Corresponding author.

https://doi.org/10.1016/j.surfin.2020.100672
Received 1 February 2020; Received in revised form 26 August 2020; Accepted 2 September 2020
Available online 11 September 2020

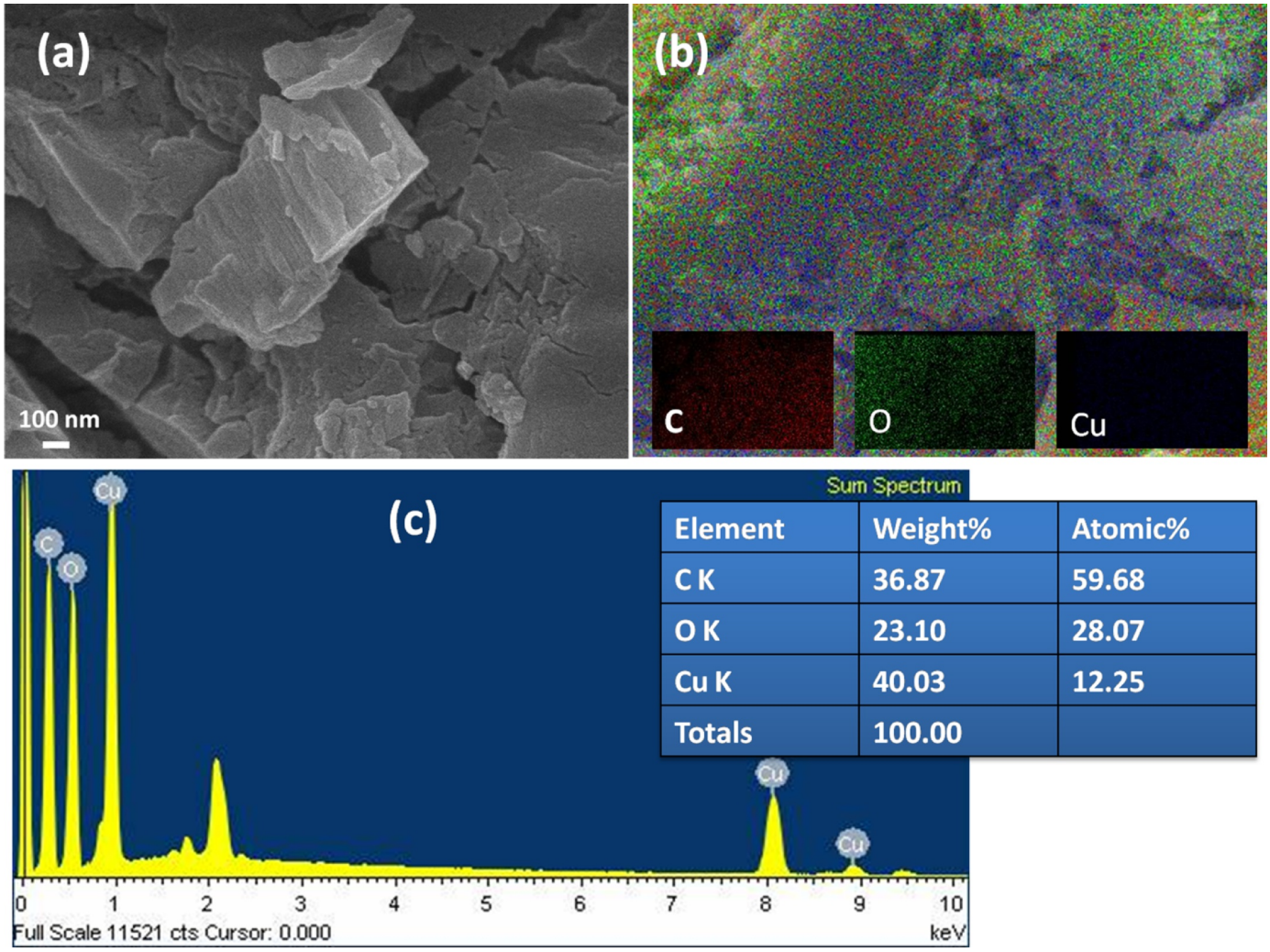

Fig. 1. (a) SEM image of Cu-BTC (b) Elemental mapping and (c) EDAX analysis of Cu-BTC.

hydrogen storage capacity exhibited by the mixtures of MOF and metal/carbons at room temperature is due to the migration of hydrogen atoms into MOF pores via catalyst (metal on MWCNTs) through spillover phenomenon [20]. But some other authors failed to attain higher uptake capacity for the composites prepared through ball-milling or physical mixing procedures. Therefore, good contact/synergistic effect between MOF and catalyst is very much essential to improve the hydrogen storage capacity [21]. In the present study, we report the hydrogen uptake capacities of nanocomposites, Cu-BTC/Ni@f-MWCNTs and Cu-BTC/Pd@f-MWCNTs along with its components such as Cu-BTC, Ni@f-MWCNTs, Pd@f-MWCNTs measured at 77 K and 298 K up to 70 bar pressure.

2. Material and methods

2.1. Synthesis of Cu-BTC

The Cu-BTC was prepared through a reported procedure by Chowdhury et al., [22]. 1,3,5-benzenetricarboxylic acid (BTC) (1.0 g) and $Cu(NO_3)_2{\cdot}3H_2O$ (2.077 g) dissolved separately in the 1:1 mixture (30 ml) of ethanol & N,N-dimethylformamide (DMF) and 15 ml of water, respectively were stirred for 10 min. The solutions were then taken into a Teflon-lined stainless steel autoclave. The mixture was hydrothermally heated for 10h at 100 °C. After Cooling slowly, the resultant blue crystals were filtered and extracted overnight with methanol using a Soxhlet extractor to remove the solvated DMF. The product was then dried at room temperature.

2.2. Preparation of Ni@f-MWCNTs and Pd@f-MWCNTs

To prepare Ni@f-MWCNTs and Pd@f-MWCNTs, 200 mg of carboxylate functionalized MWCNTs (f-MWCNTs) and 2.90 g of $Ni(NO_3)_2.6H_2O$ or 2.30 g of $Pd(NO_3)_2{\cdot}6H_2O$, mixed with 150 ml of distilled water containing 0.5 ml of triethylamine (TEA), were taken in a 500 ml round bottom flask. The above resulting clear solution, having pH is about 10.0 ± 0.2, was heated for 6 h at 80 °C. The resulting solid was thoroughly washed until the washings indicated neutral pH. The sample was dried for about 12 hours at 40 °C in vacuum.

2.3. Synthesis of nanocomposites

To prepare the nanocomposites, 200 mg of the prepared Cu-BTC, 200 mg of Ni@f-MWCNTs (for Cu-BTC/Ni@f-MWCNTs) or 200 mg of Pd@f-MWCNTs (for Cu-BTC/Pd@f-MWCNTs) were taken in a 1000 ml round bottom flask. To this, 150 ml of distilled water was added and heated thoroughly at 80 °C for 6h. The resulting solid was washed and dried overnight in vacuum at 40 °C.

2.4. Characterization

Philips CM200 (TEM) and a Zeiss Ultra plus (FEG-SEM) equipped with an EDS was used to examine the morphology of the synthesized

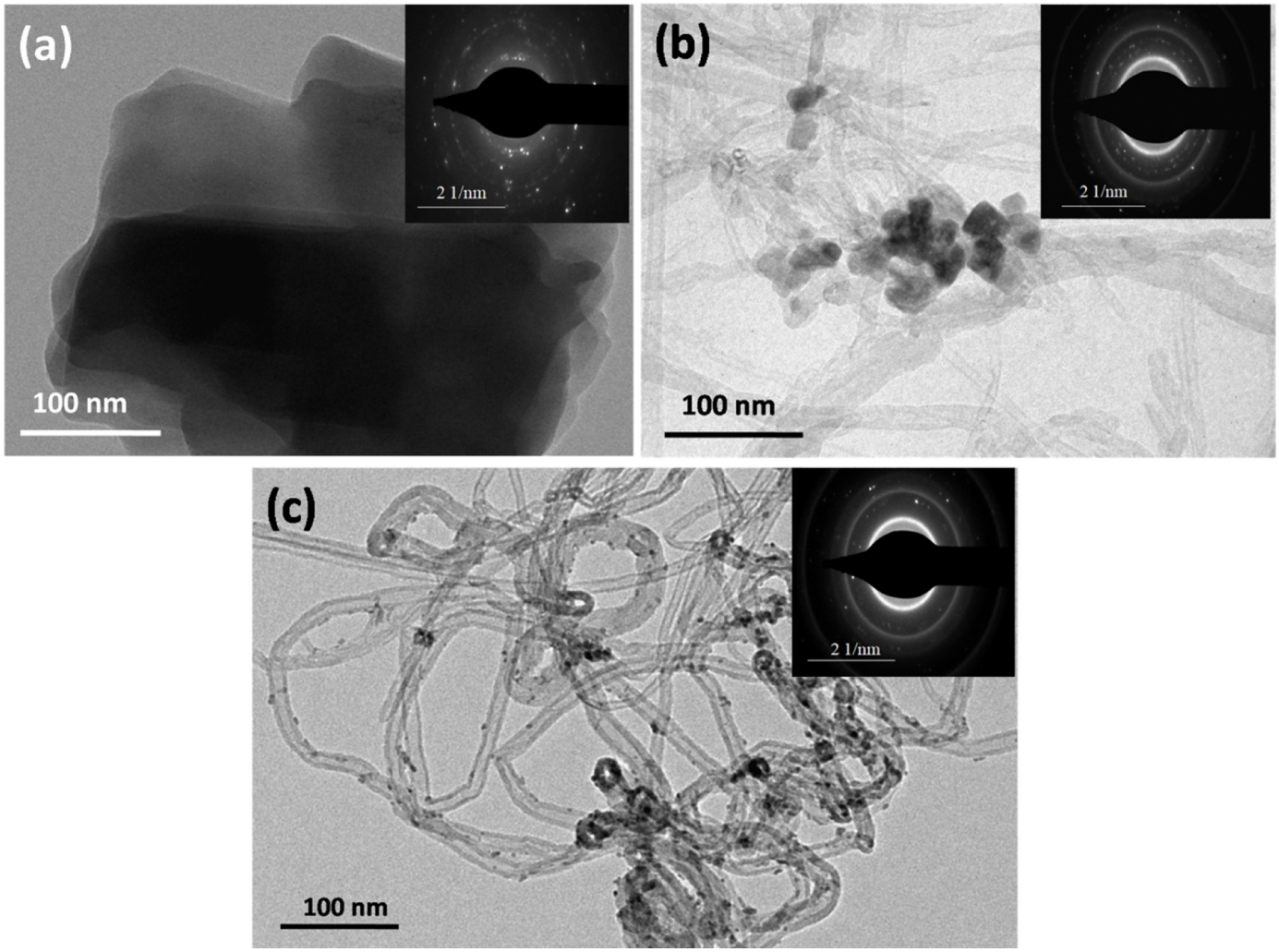

Fig. 2. (a) TEM images of (a) Cu-BTC (b) Ni@f-MWCNTs (c) Pd@f-MWCNTs (Inset: SEAD patterns).

compounds. Bruker D8 powder X-ray diffractometer (45 kV, 40 mA) with Ni-filtered Cu Ka radiation (λ = 1.5406 ˚A) was used to collect the powder X-ray diffraction patterns (XRD). The specific surface area was determined according to the Brunauer–Emmett–Teller (BET) method using Quantachrome NOVA 1200e.

2.5. Hydrogen storage capacity

BELSORP-HP was used to collect high-pressure hydrogen adsorption isotherms for the synthesized materials. Ultra-pure (99.9999%) helium and hydrogen gases were used for the measurements. The correct weight of the sample was calculated after evacuating the solvent guest molecules from the pores through activation procedure reported in the literature. Then the hydrogen uptake measurements were conducted volumetrically by varying the temperatures (77 K & 298 K) and pressures up to 70 bar.

3. Results and discussion

3.1. Morphology

The morphology and structure of Cu-BTC/Ni@MWCNTs, Cu-BTC/Pd@MWCNTs composites along with its components were examined using Scanning Electron Microscopy (SEM) and Transmission Electron Microscopy (TEM). As reported by Chowdhury et al., Cu-BTC exhibits a distinctive octahedral shaped morphology and transforms to spherically shaped particles at high-temperature synthesis [22]. Cu-BTC prepared through ultrasonic assisted hydrothermal synthesis exhibits a unique octahedral morphology [23]. SEM images of hydrothermally synthesized Cu-BTC crystals, at low temperature (100 ˚C), reveal irregular plate-like Prussian-blue colored with 500 nm to 2.0 μm size (Fig. 1). The elemental composition of Cu-BTC examined through Elemental mapping and EDAX analysis are shown in Fig. 1b and c. Metal decorated MWCNTs (Ni@f-MWCNTs or Pd@f-MWCNTs) prepared using metal precursor and carboxylate functionalized MWCNTs (f-MWCNTs) in amine (Triethylamine, TEA) solvent are shown in Fig. 2. As shown in the TEM image, Fig. 2a exhibits irregular tabular crystals of Cu-BTC with around 500nm size. The inset selected area electron diffraction (SAED) from Fig. 1a reveals that the diffraction patterns of these Cu-BTC match with the references mentioned above. TEM images from Fig. 2b and c reveal that the Ni or Pd nanoparticles are uniformly distributed on the surface of MWCNTs. Apart from aiding the uniform distribution of nanoparticles on the surface of CNTs, due to attraction of metal particles by deprotonated carboxylic acid groups, Triethylamine (TEA) solvent makes the reaction medium alkaline for better functionalization of MWCNTs and metal decoration. As shown in Fig. 2b, about 20-30 nm sized nanoparticles of Ni observed on the surface of MWCNTs. Further, in the case of Pd, tiny nanoparticles size 5-10 nm are seen on the surface of MWCNTs (Fig 2c). The selected area electron diffraction (SAED) patterns of Ni/Pd decorated MWCNTs are shown in insets of Fig. 2b and c. Our earlier reports regarding the morphology of metal decorated MWCNTs confirm the uniform distribution of

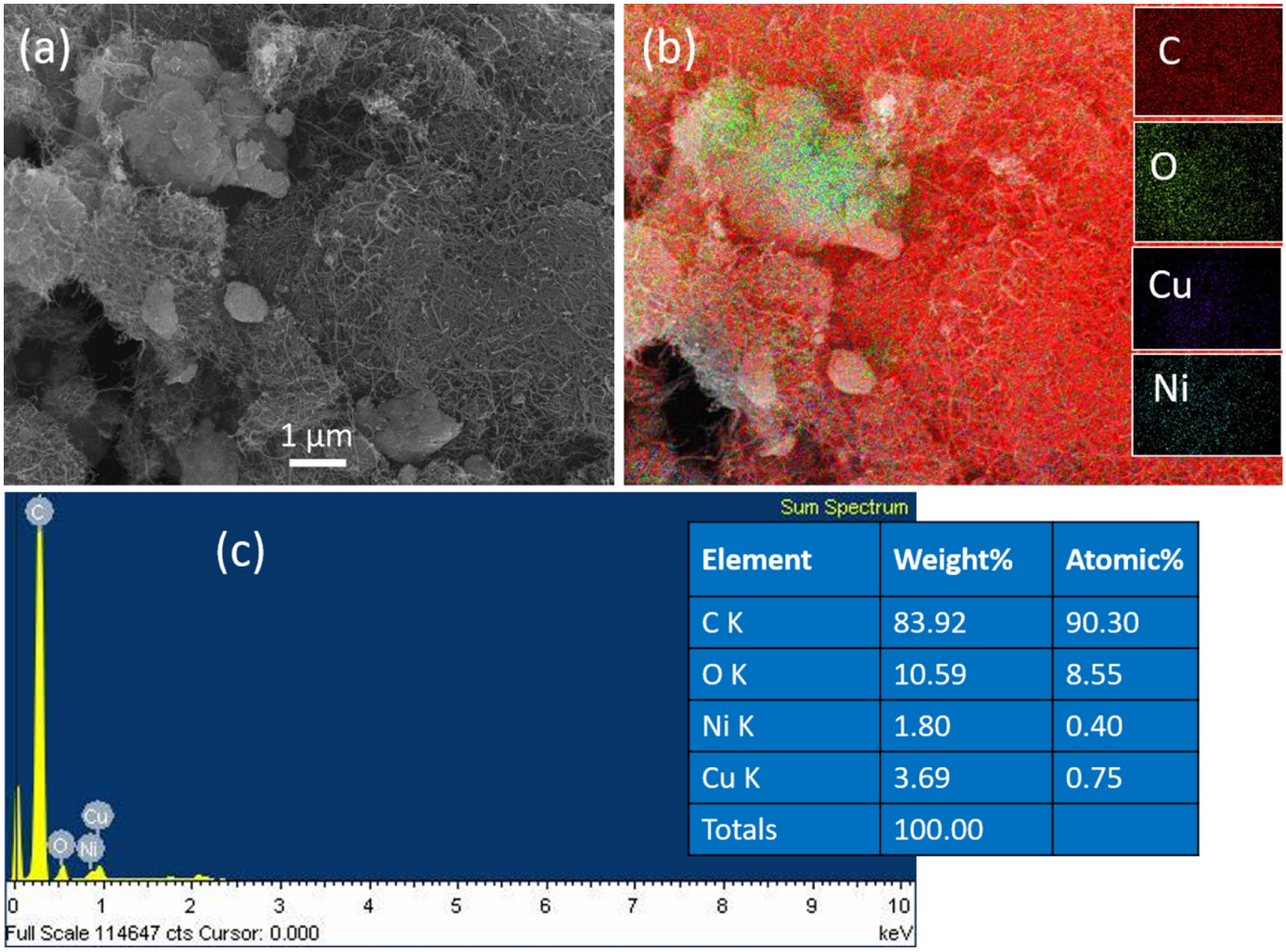

Fig. 3. (a) SEM image of Cu-BTC/Ni@MWCNTs (b) Elemental mapping and (c) EDAX analysis of Cu-BTC/ Ni@MWCNTs.

nanoparticles on CNTs prepared under similar experimental conditions using different solvents such as water, DMF and TEA [16,17].

The heterostructures of nanocomposite Cu-BTC/Ni@f-MWCNTs prepared by mixing Cu-BTC and Ni@f-MWCNTs are shown in Fig. 3. Irregular plate-like Cu-BTC seems to have transformed to a plate-like hexagonal morphology after refluxing the Cu-BTC and metal decorated MWCNTs at 95 °C in the synthesis process (Fig. 3). Clustering of CNTs around the Cu-BTC plates was observed instead of MOF being entrapped into the composite. The elemental mapping and EDAX analysis confirms the existence of Cu-BTC and Ni@MWCNTs (Fig. 3b and c). The alteration of Cu-BTC morphology is due to the chemical interaction between copper dimers from MOF and functional groups on MWCNTs [24].

Heterostructures of Cu-BTC/Pd@f-MWCNTs obtained by combining Cu-BTC and Pd@f-MWCNTs are shown in Fig. 4. The SEM image (Fig. 4a) shows that the hexagonal plates of Cu-BTC are clustered with MWCNTs. The elemental composition of the prepared composite was confirmed through elemental mapping and EDAX analysis Fig. 4b and c.

3.2. Powder XRD analysis

Powder X-ray diffraction patterns of Cu-BTC, Ni@f-MWCNTs, Pd@f-MWCNTs, Cu-BTC/Ni@f-MWCNTs and Cu-BTC/Pd@f-MWCNTs are shown in Fig. 5. The diffraction peaks at 25.4 and 42.8° correspond to the graphite reflections (JCPDS No.01-0646). The peaks at 11.6°, 19.4°, 26.4°, 29.8°, 35.3° and 39.5° are assigned to the characteristic crystal planes of Cu–BTC [25]. The peaks at 43.8° and 51.6° correspond to the nickel nanoparticles. The peaks at 33.9°, 40.1°, 46.6°, 67.9°, 82.3°,respectively correspond to the palladium nanoparticles.The above results confirm the formation of composite structures of Cu-BTC/Ni@f-MWCNTs and Cu-BTC/Pd@f-MWCNTs.

3.3. Surface area

The surface area of composite materials was examined by N_2 absorption measurements at 77 K. It reveals that the surface areas of p-MWCNTs and f-MWCNTs are 360 and 236 m^2/g, respectively. This decrease in surface area is possibly due to the blocking of pores of the p-MWCNTs by COOH functional groups after surface functionalization. On the other hand, a further decrease in surface area to 206 and 231 m^2/g is due to the decoration of metal nanoparticles of Ni and Pd, respectively, on the surface of MWCNTs. Therefore, these nanoparticles block additional surface pores of CNTs leading to further decrease in the surface area. The parent MOF material, Cu-BTC exhibits a high surface area of 1448 m^2/g. The BET surface area for composites decreases to 74 m^2/g and 172 m^2/g for Cu-BTC/Ni@f-MWCNTs and Cu-BTC/Pd@f-MWCNTs, respectively. The substantial decrease in BET surface area of the composites may be due to the decrease in the pore size of Cu-BTC and blocking of pores by agglomeration of Cu-BTC and MWCNTs [26]. Hydrogen adsorption capacity is increased with increasing surface area. Further, The BET surface area of synthesized materials is given in Table 1. In general, the adsorption of hydrogen is

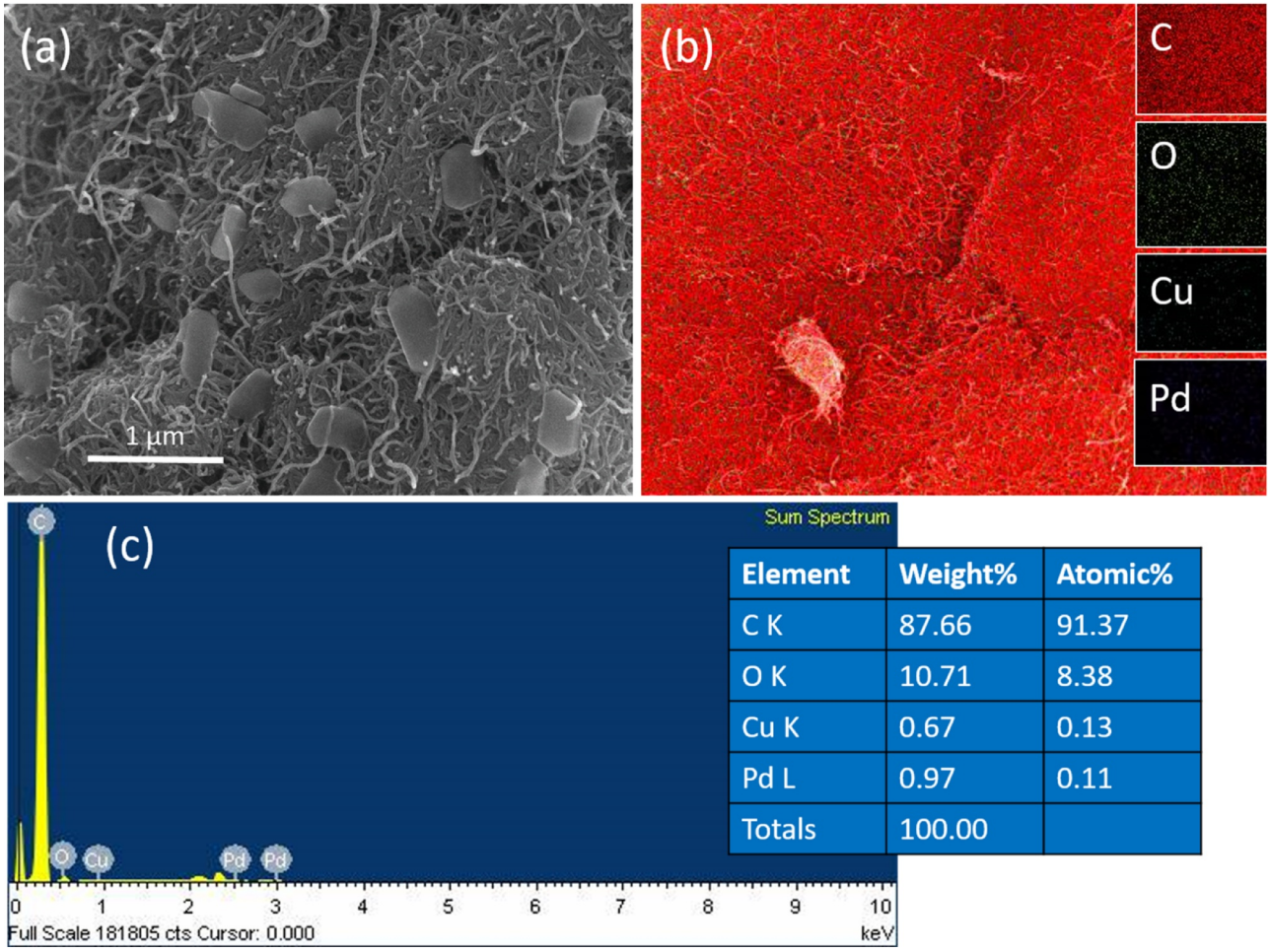

Fig. 4. (a) SEM image of Cu-BTC/Pd@MWCNTs (b) Elemental mapping and (c) EDAX analysis of Cu-BTC/ Pd@MWCNTs.

directly proportional to the surface area. The higher surface area allows more and more hydrogen into the pores of the porous materials. Furthermore, metal/metal oxides influence profoundly on adsorption behavior of hydrogen irrespective of surface area.

3.4. Hydrogen sorption analysis

The hydrogen uptake capacity of the synthesized compounds was examined volumetrically using high-pressure gas sorption analyzer BELSORP-HP at 77 K and 298 K and pressure up to 70 bar. The details of the Hydrogen storage capacity of the p-MWCNTs, f-MWCNTs, Ni@f-MWCNTs, Pd@f-MWCNTs, Cu-BTC, Cu-BTC/Ni@f-MWCNTs and Cu-BTC/Pd@f-MWCNTs, measured under above-mentioned conditions, are presented in Table 1. All the samples exhibit reversible hydrogen sorption behavior. Hence desorption curves have not been included in the figures. The excess sorption isotherms of all the samples measured at 298 K display a linear trend typical for monolayer adsorption on porous materials.

As shown in Fig. 6, p-MWCNTs and COOH-MWCNTs adsorbed 0.34 and 0.25 wt % of hydrogen, respectively measured at 77 K. The decrease in the uptake is due to blocking of pores on MWCNTs by surface functional groups (-COOH) [27]. Doping f-MWCNTs with Ni or Pd nanoparticles had a profound influence on the hydrogen uptake capacity of the synthesized materials. Metal decorated CNTs, Ni@f-MWCNTs, and Pd@f-MWCNTs adsorbed 1.87 wt% and 2.87 wt% of hydrogen, respectively, at 77 K (Fig. 6c and d). On the other side, Cu-BTC adsorbed 3.0 wt % under similar conditions (Fig. 6e). As shown in Fig. 6f and g, the hydrogen storage capacity is enhanced to 4.68 wt% and 5.31 wt% for composites of Cu-BTC/Ni@f-MWCNTs and Cu-BTC/Pd@f-MWCNTs, respectively at 77 K and 70 bar.

As shown in hydrogen uptake curves, p-MWCNTs and COOH-MWCNTs adsorbed 0.12 and 0.06 wt % of hydrogen, respectively, at 298 K and 70 bar (Fig. 7a and b). Further, Ni@f-MWCNTs, Pd@f-MWCNTs, and Cu-BTC had exhibited hydrogen sorption of about 0.97, 1.36, and 0.36 wt%, respectively under identical conditions (Fig. 7c and d). Furthermore, composites of Cu-BTC/Ni@f-MWCNTs and Cu-BTC/Pd@f-MWCNTs adsorbs 1.29 and 1.67 wt %, respectively, at 298 K and 70 bar pressure (Fig 7f and g). Yang et al., proposed the spillover approach for hydrogen storage based on experimental results and molecular orbital calculations [28]. According to this mechanism, molecular hydrogen adsorbed initially on Ni or Pd metal/nanoparticles dissociates into atomic hydrogen which subsequently migrates to spillover receptor, CNT. This process possibly enhances the hydrogen storage. In case of the composites, the hydrogen storage capacity of carbon materials is further increased by secondary spillover mechanism [29]. Through bridge-building technique wherein (secondary spillover) the hydrogen atoms adsorbed on the CNTs by the first spillover process are further transferred to the surface of MOFs. A similar observation was found in the present study also. It was observed that the overall hydrogen uptake had profoundly enhanced, through the primary and secondary spillover mechanism, for the nanocomposites prepared from Ni@f-MWCNTs or Pd@f-MWCNTs with Cu-BTC.

Rapid adsorption/desorption kinetics and adequate multicycle stability are required for onboard applications of hydrogen-powered vehicles. Hence, multi-cycle dsorption/desorption of hydrogen by Cu-BTC/Ni@f-MWCNTs had also been examined at 298 K (Fig. 8). Cu-BTC/

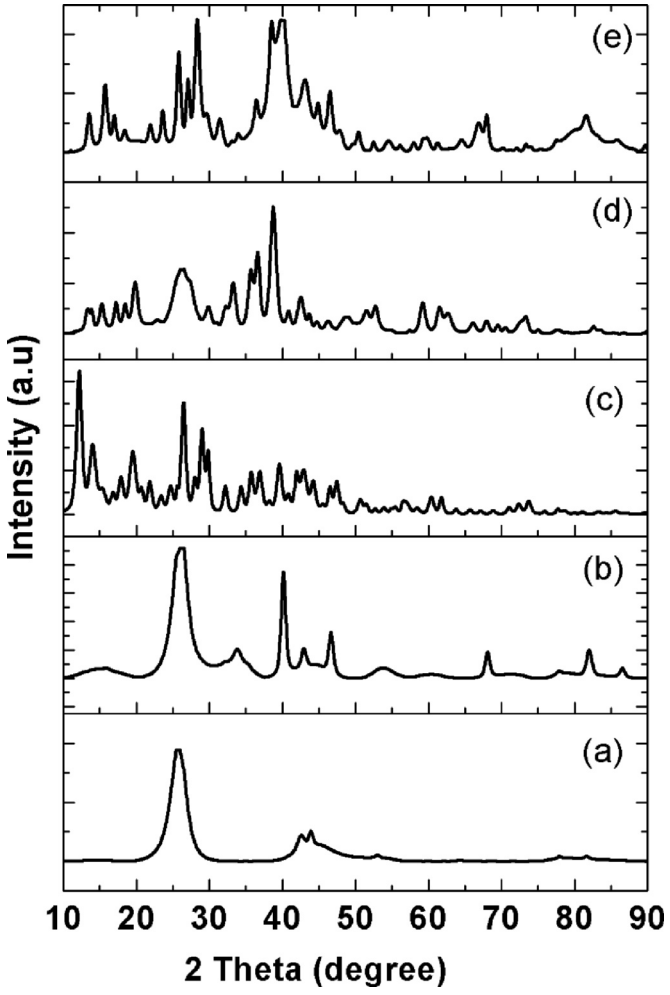

Fig. 5. Powder diffraction patterns of (a) Ni@f-MWCNTs (b) Pd@f-MWCNTs (c) Cu-BTC (d) Cu-BTC/Ni@f-MWCNTs, (e) Cu-BTC/Pd@f-MWCNTs.

Table 1
BET Surface area and hydrogen uptake capacity of synthesized composites.

Sample	^{s}BET (m^2/g)	H_2 uptake at 298 K & 70 bar (wt %)	H_2 uptake at 77 K & 70 bar (wt %)
p-MWCNT	360	0.12	0.34
f-MWCNT	236	0.06	0.25
Cu-BTC	1448	0.36	3.01
Ni@f-MWCNT	206	0.97	1.87
Pd@f-MWCNT	231	1.36	2.87
Cu-BTC/Ni@f-MWCNT	74	1.29	4.68
Cu-BTC/Pd@f-MWCNT	172	1.67	5.31

Ni@f-MWCNTs exhibit excellent cyclic stability even after 7 cycles.

4. Conclusions

In the present paper, we report synthesis, morphology, and hydrogen uptake behavior of Cu-BTC/Ni@f-MWCNTs and Cu-BTC/Pd@f-MWCNTs along with the parent materials Ni@f-MWCNTs, Pd@f-MWCNTs and Cu-BTC. The hydrogen uptake by the Cu-BTC/Ni@f-MWCNTs and Cu-BTC/Pd@f-MWCNTs was enhanced up to 2 fold at 77K and 2-3 fold at 298 K. So impregnating metal nanoparticles on CNTs and surface area of MOF in composites played key roles for the higher uptake of hydrogen through primary and secondary spillover via bridge-building technique. Moreover, the multi-cycle adsorption/desorption of hydrogen reveals that the Cu-BTC/Ni@f-MWCNTs loses only 6 % efficiency after seven cycles.

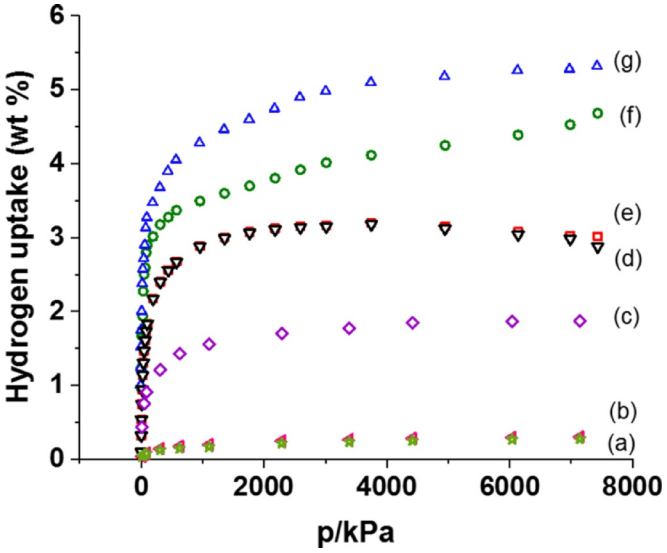

Fig. 6. Hydrogen uptake capacities of (a) p-MWCNTs (b) f-MWCNTs (c) Ni@f-MWCNTs (d) Pd@f-MWCNTs (e) Cu-BTC (f) Cu-BTC/Ni@f-MWCNTs (g) Cu-BTC/Pd@f-MWCNTs at 77 K.

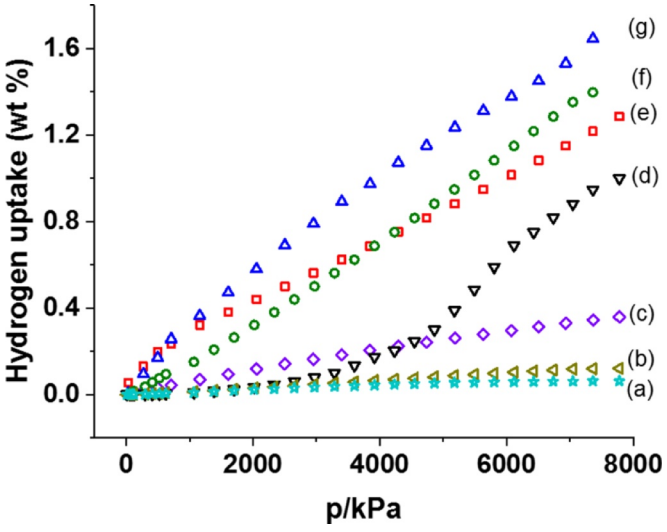

Fig. 7. Hydrogen uptake capacities of (a) p-MWCNTs (b) f-MWCNTs (c) Cu-BTC (d) Ni@f-MWCNTs (e) Cu-BTC/Ni@f-MWCNTs (f) Pd@f-MWCNTs (g) Cu-BTC/Pd@f-MWCNTs at 298 K.

Author statement

This manuscript is the authors' original work and has not been published nor has it been submitted simultaneously elsewhere. I am herewith submitting the manuscript along with necessary information for your kind consideration.

We confirm that the manuscript has been read and approved by all named authors and that there are no other persons who satisfied the criteria for authorship but are not listed. We further confirm that the order of authors listed in the manuscript has been approved by all of us.

We understand that the Corresponding Author is the sole contact for the Editorial process. He/she is responsible for communicating with the other authors about progress, submissions of revisions and final approval of proofs

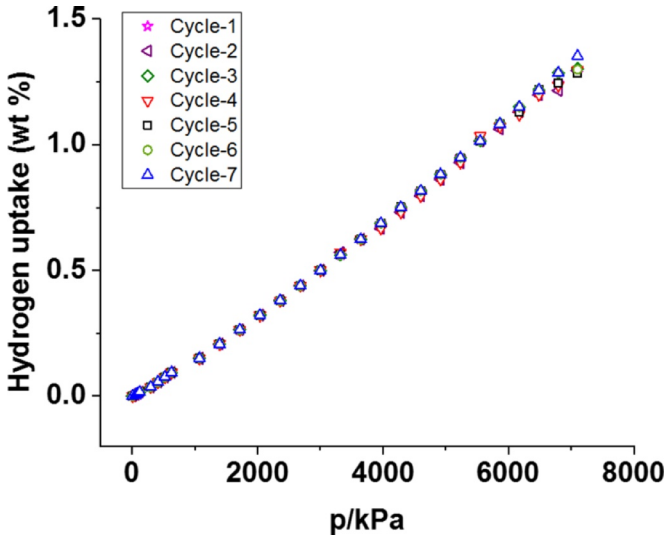

Fig. 8. Cycle life performance of Cu-BTC/Ni@f-MWCNTs at 298 K.

Declaration of Competing Interest

The authors declare that they have no known competing financial interests or personal relationships that could have appeared to influence the work reported in this paper.

Acknowledgments

This work was supported by the University Grants Commission (UGC), Govt. of India (Project No: 42-258/2013 (SR)). The authors sincerely acknowledge the SAIF, IIT Bombay, for assistance with SEM and TEM measurements

Supplementary materials

Supplementary material associated with this article can be found, in the online version, at doi:10.1016/j.surfin.2020.100672.

References

[1] A. Canan, D. Ibrahim, The potential role of hydrogen as a sustainable transportation fuel to combat global warming, Int. J. Hydrogen Energy 45 (2020) 3396–3406.
[2] M. Jacoby, MOF boasts impressive gas-storage properties, ACS C&EN Global Enterprise 98 (2020) 5.
[3] E. Klontzas, E. Tylianakis, G.E. Froudakis, On the enhancement of molecular hydrogen interactions in nanoporous solids for improved hydrogen storage, J. Phys. Chem. Lett. 2 (2011) 1824–1830.
[4] U. S. Department of Energy (DOE) technical targets for onboard hydrogen storage for light-duty vehicles (https://www.energy.gov/eere/fuelcells/doe-technical-targets-onboard-hydrogen-storage-light-duty-vehicles).
[5] M. Hirscher, B. Panella, B. Schitz, Metal-organic frameworks for hydrogen storage, Microporous Mesoporous Mater. 129 (2010) 335–339.
[6] A. Ahmed, S. Seth, J. Purewal, A.G. Wong-Foy, M. Veenstra, A.J. Matzger, D.J. Siegel, Exceptional hydrogen storage achieved by screening nearly half a million metal-organic frameworks, Nature Commun. 10 (2019) Article No.1568.
[7] M.T. Kapelewski, T. Runevski, J.D. Tarver, H.Z.H. Jiang, K.E. Hurst, P.A. Parilla, A. Ayala, T. Gennett, S.A. FitzGerald, C.M. Brown, J.R. Long, Record high hydrogen storage capacity in the metal−organic framework Ni_2(m-dobdc) at near-ambient temperatures, Chem. Mater. 30 (2018) 8179–8189.
[8] S.S.Y. Chui, S.M.F. Lo, J.P.H. Charmant, A.G. Orpen, I.D. Williams, A chemically functionalizable nanoporous material, Science 283 (1999) 1148–1150.
[9] J.Y. Lee, D.H. Olson, L. Pan, T.J. Emge, J. Li, Microporous metal-organic frameworks with high gas sorption and separation capacity, Adv. Fun. Mater. 17 (2007) 1255–1262.
[10] B. Panella, M. Hirscher, S. Roth, Hydrogen adsorption in different carbon nanostructures, Carbon 43 (2005) 2209–2214.
[11] A. Rehman, S.A. Tirmizi, A. Badshah, H.M. Ammad, M. Jawad, S.M. Abbas, U.A. Rana, S.U. Khan, Synthesis of highly stable MOF-5@MWCNTs nanocomposite with improved hydrophobic properties, Arabian J. Chem. 11 (2018) 26–33.
[12] A. Reyhani, S.Z. Mortazavi, S. Mirershadi, A.Z. Moshfegh, P. Parvin, A.N. Golikand, Hydrogen storage in decorated multiwalled carbon nanotubes by Ca, Co, Fe, Ni, and Pd nanoparticles under ambient conditions, J. Phys. Chem. C 115 (2011) 6994–7001.
[13] I.K. Petrushenko, K.B. Petrushenko, Hydrogen physisorption on nitrogen-doped graphene and graphene-like boron nitride-carbon heterostructures: a DFT study, Surf. Interfaces 17 (2019) Article 100355.
[14] M. Aghababaei, A.A. Ghoreyshi, K. Esfandiari, Optimizing the conditions of multi-walled carbon nanotubes surface activation and loading metal nanoparticles for enhanced hydrogen storage, Int. J. Hydrogen Energy 45 (2020) 23112–23121.
[15] K. Madhavi, N. Narayanam, A.S. Dadhich, S.B. Mukkamala, Effect of Reaction media on hydrogen sorption properties of Mg-decorated MWCNTs, Fullerenes Nanotubes Carbon Nanostruct. 23 (2015) 782–787.
[16] K. Madhavi, A.S. Dadhich, S.B. Mukkamala, Impact of surface modifications on hydrogen uptake by Fe@f-MWCNTs and Cu@f-MWCNTs at non-cryogenic temperatures, Int. J. Hydrogen Energy 42 (2017) 953–959.
[17] K. Madhavi, A.S. Dadhich, S.B. Mukkamala, Solvent induced surface modifications on hydrogen storage performance of ZnO nanoparticle decorated MWCNTs, Sustain. Energy Fuels 2 (2018) 466–471.
[18] S.Z. Mortazavi, P. Parvin, A. Reyhani, R. Malekfar, S. Mirershadi, Hydrogen storage property of laser induced Pd-nanoparticle decorated multi-walled carbon nanotubes, RSC Adv. 3 (2013) 1397–1409.
[19] J. Shi, W. Li, D. Li, Synthesis, nickel decoration, and hydrogen adsorption of silica-templated mesoporous carbon material with high surface area, J. Phys. Chem. C 119 (2015) 23430–23435.
[20] G. Blanita, M. Mihet, G. Borodi, I. Misan, I. Coldea, D. Lupu, Ball milling and compression effects on hydrogen adsorption by MOF:Pt/carbon mixtures, Microporous Mesoporous Mater. 203 (2015) 195–201.
[21] K. Esfandiari, A.R. Mahdavi, A.A. Ghoreyshi, M. Jahanshahi, Optimizing parameters affecting synthesize of Cu-BTC using response surface methodology and development of AC@Cu-BTC composite for enhanced hydrogen uptake, Int. J. Hydrogen Energy 43 (2018) 6654–6665.
[22] P. Chowdhury, C. Bikkina, D. Meister, F. Dreisbach, S. Gumma, Comparison of adsorption isotherms on Cu-BTC metal organic frameworks synthesized from different routes, Microporous Mesoporous Mater. 117 (2009) 406–413.
[23] R. Kaur, A. Kaur, A. Umar, W.A. Anderson, S.K. Kansal, Metal organic framework (MOF) porous octahedral nanocrystals of Cu-BTC: synthesis, properties and enhanced absorption properties, Mat. Res. Bull. 109 (2018) 124–133.
[24] Z. Hu, X. Liu, J. Zhang, X. Yan, Y. Liu, A. Yuan, Enhanced room-temperature hydrogen storage capacity in Pt-loaded graphene oxide/HKUST-1 composites, Int. J. Hydrogen Energy 39 (2014) 2160–2167.
[25] R.M.H. Abdelhameed, M.Elshahat Abdel-Gawada, H.E. Emam, Cu–BTC@cotton composite: design and removal of ethion insecticide from water, RSC Adv. 6 (2016) 42324–42333.
[26] E. Zhou, Y. Zhang, Y. Li, X. He, Cu(II)-based MOF immobilized on multiwalled carbon nanotubes: synthesis and application for non enzymatic detection of hydrogen peroxide with high sensitivity, Electroanalysis 26 (2014) 2526–2533.
[27] M. Allegri, D.K. Perivoliotis, M.G. Bianchic, M. Chiu, A. Pagliaro, M.A. Koklioti, A.F. Trompeta, E. Bergamaschi, O. Bussolati, C.A. Charitidis, Toxicity determinants of multi-walled carbon nanotubes: the relationship between functionalization and agglomeration, Toxicol. Rep. 3 (2016) 230–243.
[28] Yang F.H, R.T.Yang F.H., Ab initio molecular orbital study of adsorption of atomic hydrogen on graphite: insight into hydrogen storage in carbon nanotubes, Carbon 40 (2002) 437–444.
[29] A.J. Robell, E.V. Ballou, M. Boudart, Surface diffusion of hydrogen on carbon, J. Phys. Chem. 68 (1964) 2748–2753.